MARS SUBSURFACE WATER ICE MAPPING (SWIM): THERMAL ANALYSIS. R. H. Hoover,[1] H. G. Sizemore,[2] Z. Bain[2], N. E. Putzig,[2] G. A. Morgan[2], M. R. Perry[2], M. Mastrogiuseppe[3], D. M. H. Baker[4], A. M. Bramson[5], E. Petersen[5], I. B. Smith,[2] B. A. Campbell.[6] [1]Southwest Research Institute (RHoover@boulder.swri.edu), [2]Planetary Science Institute, [3]California Institute of Technology, [4]NASA Goddard Space Flight Center, [5]University of Arizona Lunar and Planetary Laboratory, [6]Smithsonian Institution.

Introduction: The Mars Subsurface Water Ice Mapping (SWIM) project aims to increase our current knowledge regarding the presence, location, depth and concentration of subsurface ice on Mars. Our project actively integrates subsurface detections of ice from 0º–60ºN within four broad longitude ranges: "Arcadia" (150-225ºE, which also contains our pilot study region), "Acidalia" (290-360ºE), "Onilus" (0-70ºE) and "Utopia" (70-150ºE). Ice has previously been identified at varying depths in these regions using several techniques and instruments (Fig. 1). For example, the Mars Odyssey Neutron Spectrometer (MONS) identified water-equivalent hydrogen, which is thought to indicate the presence of subsurface ice in the form of water-bearing soils [1]. These findings were corroborated by thermal analysis using data from the Mars Global Surveyor Thermal Emissions Spectrometer (TES) and numerical models of ground ice stability [2].

More recent evidence of ice has been identified in small, fresh impact craters which expose ice within the upper 1 m of the surface, e.g., [3], [4]. Geomorphic analysis, specifically identification of features such as lobate debris aprons, polygonal terrain, degraded mantles, and solifluction lobes has been used to identify the presence of near-surface or deep ice, e.g., [5], [6], [7]. Building upon this previous work, the SWIM project combines the use of several techniques (radar, geomorphology, and thermal analyses) to make a comprehensive evaluation of our confidence in the presence of ice throughout the study regions. Although the larger SWIM project combines several techniques, the results presented here focus on the thermal analysis.

The SWIM Equation: We introduce the SWIM Equation, in the spirit of the Drake Equation [8], to evaluate how consistent (or inconsistent) the presence of shallow (<5 m) and deep (>5 m) ice is across these regions in the numerous remote-sensing datasets. The SWIM Equation is outlined in detail by Perry et al. [this LPSC]. Consistency values range between +1 and -1, where: +1 means that the data are consistent with the presence of ice, 0 means that the data gives no indications of presence or absence of ice, and -1 means that the data are inconsistent with the presence of ice. In this abstract, we focus on our assessment of ice consistency for the thermal analysis associated with the presence of shallow ice. For more information regarding the SWIM project and its techniques and datasets, visit our website (swim.psi.edu) and see the other SWIM Project abstracts this LPSC: Morgan at al. (overview), Bramson et al. (subsurface radar), Perry et al. (infrastructure), Bain et al. (surface radar), and Putzig et al. (geomorphology). You can also follow us follow @RedPlanetSWIM on Twitter for project news and product release information.

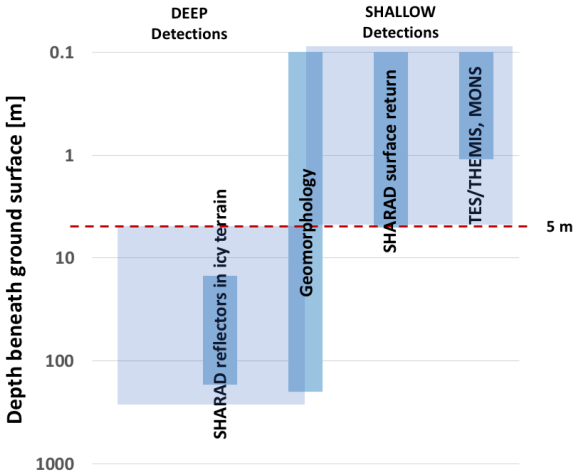

Fig. 1. Summary of depth ranges and analysis types in the SWIM project. This abstract focuses on TES and THEMIS thermal data.

Thermal Analysis: The thermal properties of a material, which are influenced by grain size, distribution, induration and rock abundance [9], can be used to identify surface materials and subsurface volatiles, e.g., [10], [11]. We employ data from TES and the Mars Odyssey Thermal Imaging System (THEMIS) to identify the material layering consistent with ice in the upper 1 m of the near surface.

Our technique exploits seasonal variations in apparent thermal inertia (ATI), to derive information about the heterogeneity of the Martian surface [10, 12]. ATI is derived from orbital brightness temperatures, using homogeneous models of subsurface thermal behavior. As a result, ATI exhibits diurnal and seasonal variations when material heterogeneities are present in the field of view [13], [14]. By comparing observed variation in ATI to that from numerical models of heterogeneous surfaces, we can distinguish layering and horizontal mixing of different materials (e.g., dust, sand, duricrust, and 'rock,' where rock is thermally indistinguishable from ice and ice-cemented soil).

Using TES-derived ATI, we have created a global layered-surface heterogeneity map, which improves the resolution and coverage of the previous global map [12] and identifies the best two-component layered-model types at each pixel. Producing a similar global THEMIS product is time prohibitive and is challenging due to the lack of useful dayside observations. We have selected 6-8 locations in each SWIM study region for THEMIS

analysis, which uses nighttime data only (daytime data are not useful for ATI). We convert heterogeneity matches in our TES and THEMIS maps to "ice confidence" values for integration into the SWIM equation [15].

Results: Here we present interim results at the time of submission, which include our TES global map and focused TES and THEMIS analyses in a pilot study region of Aracadia Planitia. At the 50th LPSC, we will present maps displaying heterogeneity types for each study region. Fig. 2 shows TES global heterogeneity map at 1.25º per pixel. Blue and green pixels are consistent with the presence of ice and are assigned a consistency value of 1. Fig. 3 shows heterogeneity maps derived from TES and THEMIS in the pilot study region (0-60° N, 188-202° E).

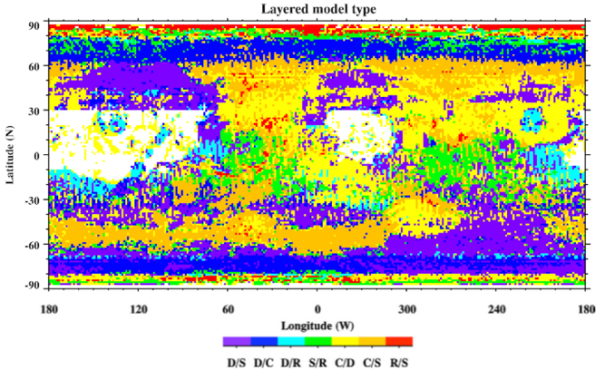

Fig. 2: Global map of TES two-layer heterogeneity model matches 1.25° per pixel. Materials in models are D: dust, S: sand, C: duricrust, and R: rock/ice.

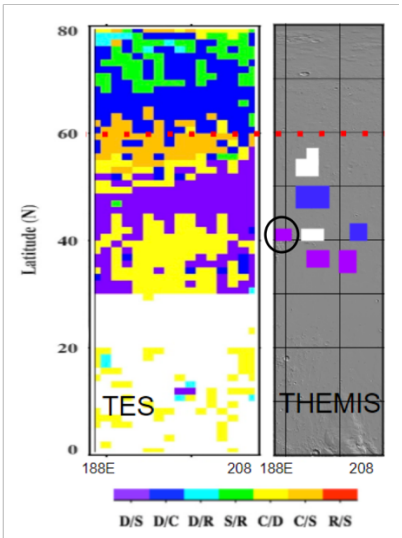

Fig. 3: TES (left) and THEMIS (right) two-layer heterogeneity map for the Arcadia pilot swath.

Fig. 2 shows the global trends: blue and green pixels are prevalent poleward of 60ºN, indicating a low thermal inertia layer overlaying a high thermal inertia layer, consistent with buried ice. In Arcadia (Fig. 3), subsurface ice is also identified poleward of 60ºN as well as in several other locations between 30-60ºN, again represented in the green and blue pixels. Eight areas within Arcadia were selected for further thermal analysis with THEMIS data (Fig. 3).

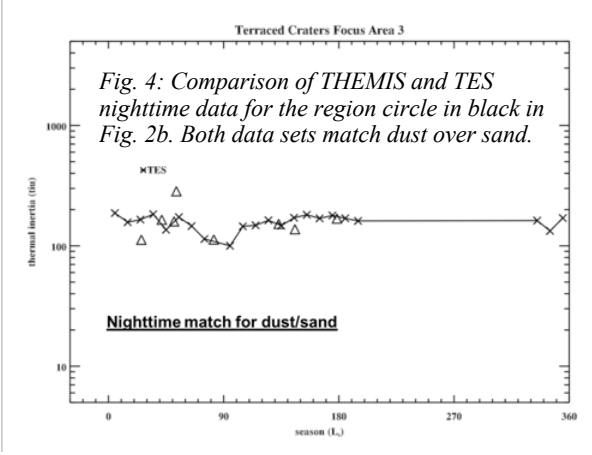

Fig. 4: Comparison of THEMIS and TES nighttime data for the region circle in black in Fig. 2b. Both data sets match dust over sand.

Within these eight regions, we compared THEMIS and TES heterogeneity matches (e.g., Fig. 4). Fig. 3 indicates five areas where THEMIS and TES results match (blue and purple pixels), two of which potentially identify ice (blue), while in two of the areas investigated, THEMIS and TES results do not match (white).

Discussion: Our TES global two-layer heterogeneity map improves resolution from 5º [12] to 1.25º per pixel, allowing for a more precise identification of subsurface ice. Comparison of THEMIS and TES model results identifies areas in which the thermal data indicate layering consistent with shallow ice between 40ºN and 60ºN. Inconsistencies between the TES and THEMIS results arise from the exclusive use of nighttime data in the THEMIS analysis, whereas the TES analysis requires consistency between daytime and nighttime heterogeneity models. Subsequent mapping will separate daytime and nighttime TES analysis, which will allow for a more direct comparison with THEMIS. Future work for the thermal portion of the SWIM project will be expanded to include all four longitudinal areas of interest.

Acknowledgments: The SWIM project is supported by NASA through JPL Subcontract 1611855.

References: [1] Feldman W.C. et al. (2004) JGR 109, 13. [2] Mellon M.T. et al. (2004) Icarus 169, 324-340. [3] Byrne S. et al. (2009) Science 325, 1674. [4] Dundas C. et al. (2013) Science, 359 199-201. [5] Head J.W. et al. (2003) Nature 426, 797-802. [6] Head J.W. et al. (2005) Nature 434, 346-351. [7] Morgan G.A. et al. (2009) Icarus 202, 22-38. [8] Drake F. and Sobel D. (1992) ISBN 0-385-31122-2. [9] Mellon M.T. et al. (2000) Icarus 148, 437-455. [10] Putzig N.E. et al. (2014) Icarus 230, 64-76. [11] Hoover R.H. et al., (2018) LPSC Abs. #1811. [12] Putzig, N.E. and Mellon, M.T. (2007) Icarus 191, 68-94. [13] Mellon M.T. et al. (2008) in: Bell J. F., ed. (2008) Cambridge U. Press. [14] Putzig N. E. and Mellon M. T. (2007) Icarus 191, 52-67.